Available online at www.sciencedirect.com
SCIENCE DIRECT
Journal of Sound and Vibration 297 (2006) 351–364
JOURNAL OF SOUND AND VIBRATION
www.elsevier.com/locate/jsvi

Free vibration of long-span continuous rectangular Kirchhoff plates with internal rigid line supports

C.F. Lü[a,b], Y.Y. Lee[c], C.W. Lim[c], W.Q. Chen[a,b,*]

[a]*Department of Civil Engineering, Zhejiang University, Hangzhou 310027, PR China*
[b]*State Key Lab of CAD & CG, Zhejiang University, Hangzhou 310027, PR China*
[c]*Department of Building and Construction, City University of Hong Kong, Kowloon, Hong Kong, PR China*

Received 10 September 2005; received in revised form 14 February 2006; accepted 10 April 2006
Available online 27 June 2006

Abstract

Exact analysis for free vibration of long-span continuous rectangular plates is presented based on the classical Kirchhoff plate theory, using the state space approach associated with joint coupling matrices. Lévy-type solution is adopted to model the field variation in the direction perpendicular to the pair of simply supported edges. The series of internal rigid line supports are parallel to the remaining pair of edges, which can be of an arbitrary combination of simply supported, clamped and free edges. Transfer relationship is derived in the span direction by the state space approach. The joint coupling matrices are employed to avoid numerical instability that exists in the conventional state space approach for high-frequency calculation or long-span geometry. Numerical calculation is carried out to validate effectiveness and efficiency of the present method. Influence of location of internal line supports on natural frequencies of multi-span plates with large aspect ratios is investigated and discussed.

1. Introduction

Multi-span rectangular plates have been encountered in various engineering fields including civil, mechanical, naval, aerospace and marine structures. Concrete applications include multi-span highway bridges, continuous viaducts, steel bridge deck of oversea bridges, long-span roofs, etc. Free vibration of such structures has been an intensive research focus for several decades because knowledge of natural frequencies helps to avoid resonance excited by moving traffic, operating machinery, wind loads and seismic dynamic loads.

Holzer's method was employed by Veletsos and Newmark [1], who presented the first investigation of rectangular plates, which are continuous over internal straight rigid supports normal to two opposite hinged edges. A semi-graphical method was proposed by Ungar [2] to study the free vibration of two-span, simply supported plates. Dickinson and Warburton [3] used the edge effect method, which permits treatment of clamped continuous edges, to determine natural frequencies of two-span plates. Cheung and Cheung [4] used the finite-strip method with single-span beam functions to study the vibration behavior of continuous plates, while plates continuous in one or two directions were investigated by Wu and Cheung [5]. The finite strip element method was

*Corresponding author. Tel.: +86 571 87952284; fax: +86 571 87952165.
E-mail addresses: chenwq@ccea.zju.edu.cn, chenwq@rocketmail.com (W.Q. Chen).

0022-460X/$ - see front matter © 2006 Elsevier Ltd. All rights reserved.
doi:10.1016/j.jsv.2006.04.007

later used by Golley and Petrolito [6] for dynamic analysis of orthotropic plates with internal point or line supports. Sakata [7] used the reduction formula to get the natural frequency and buckling force of an orthotropic continuous plate subject to bi-axial in-plane forces. Takahashi and Chishaki [8] developed an analytical method to determine the vibration characteristics of rectangular plates continuous in two directions. Azimi et al. [9] applied the receptance method developed by Bishop and Johnson [10] to analyze the free vibration of thin rectangular plates continuous over intermediate rigid simple supports and simply supported along two opposite edges. The calculation of fundamental frequency of continuous plates using simple polynomial coordinate functions and the Rayleigh–Schmidt method was suggested by Cortinez and Laura [11]. Kim and Dickinson [12] employed the Rayleigh–Ritz method to study the problems of flexural vibration of thin rectangular continuous plates. Numerical results were given for plates having various combinations of boundary conditions and various numbers of spans in one or two directions and for a particular four-span cantilevered box. Natural frequencies of multi-span plates were reported by Liew and Lam [13] using a set of orthogonally generated two-dimensional plate functions, while the vibration of rectangular Mindlin plates with internal line supports either in parallel or in diagonal directions was studied by Liew et al. [14] using the Ritz method. To cater for internal line supports, Zhou [15] used appropriate polynomials by modifying the single-span vibrating beam functions, and Kong and Cheung [16] combined Zhou's trial functions with the finite layer method to determine the frequency parameters of shear-deformable plates with internal line supports. Wei et al. [17] developed the discrete singular convolution algorithm for vibration analysis of rectangular plates with partial internal line supports. For multi-span rectangular thin plates with two opposite edges simply supported, Xiang et al. [18] used the Lévy-type solution to conduct an exact vibration analysis, in which they derived a set of first-order ordinary differential equations with respect to the plate deflection and its derivatives, and a system of linear equations was obtained by grouping all together the boundary conditions at the other two edges and conditions at the internal line supports.

In this paper, free vibration of long-span continuous rectangular Kirchhoff plates is investigated using the state space approach (transfer matrix method) in conjunction with joint coupling matrices. The series of internal rigid line supports, which are the constraints of zero transverse displacement, are perpendicular to the pair of simply supported edges. The remaining two edges can be of an arbitrary combination of simply supported, clamped and free edges. Although the problem is similar to that considered by Xiang et al. [18], the analysis is different in principle. First, the state equation is derived with state vector composed of deflection, slop, moment and equivalent shear force, which facilitate precise expression of boundary conditions and internal line support conditions. Second, the joint coupling matrices concept proposed by Nagem and Williams [19] is adopted to establish the frequency equation of plate. This is particularly important for prevention of numerical instability associated with the conventional state space approach (transfer matrix method) when the frequency is very high or the plate span is very large. Numerical examples are presented to validate effectiveness and efficiency of the present method. Effect of the location of internal line supports on the natural frequencies of multi-span plates with large aspect ratios is investigated.

2. State equation and solution

A multi-span rectangular isotropic plate with uniform thickness h is depicted in Fig. 1. The plate is of width a, length b, Young's modulus E, and Poisson's ratio v. The x-and y-axis coincide with edges OA and OB, respectively, while the origin is at the joint of the edges. Capital letters $(J, K, L, \ldots)$ are used to represent the individual spans. The left edge of a typical span, say the Kth span that is of length b_K, is designated as the Kth line support. For the plate considered, the pair of opposite edges OB and AC are simply supported, while the remaining two edges are of general supports. Further, the plate has p spans and $(p-1)$ internal line supports which require constraints of zero transverse displacement along the line supports.

2.1. Basic equations

In free vibration, the governing equations for an individual span of Kirchhoff plate are as follows:

$$\frac{\partial Q_x}{\partial x}+\frac{\partial Q_y}{\partial y}=\rho h\frac{\partial^2 w}{\partial t^2},\quad \frac{\partial M_x}{\partial x}+\frac{\partial M_{xy}}{\partial y}-Q_x=0,\quad \frac{\partial M_{xy}}{\partial x}+\frac{\partial M_y}{\partial y}-Q_y=0, \tag{1}$$

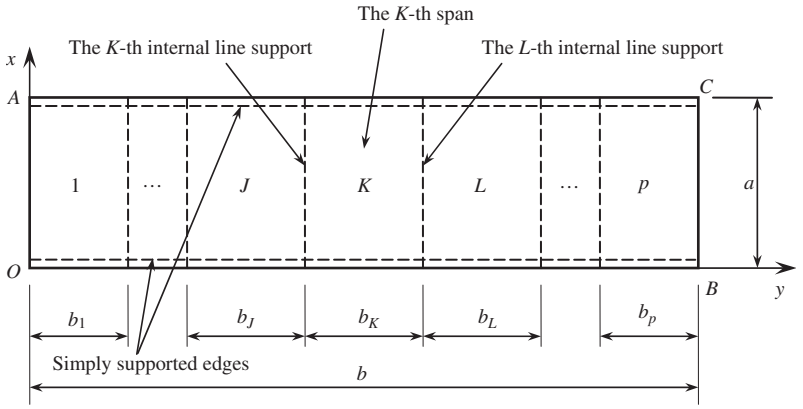

Fig. 1. Geometry of a rectangular plate with internal line supports.

where ρ and w are, respectively, the material density and transverse displacement (deflection), Q_x and Q_y are the transverse shear forces, M_x and M_y the bending moments, and M_{xy} the twisting moment. These resultant quantities, defined as the forces and moments per unit length of the section on which they act, can be expressed in terms of the transverse displacement as

$$M_x = -D\left(\frac{\partial^2 w}{\partial x^2} + v\frac{\partial^2 w}{\partial y^2}\right), \quad M_y = -D\left(v\frac{\partial^2 w}{\partial x^2} + \frac{\partial^2 w}{\partial y^2}\right), \quad M_{xy} = -(1-v)D\frac{\partial^2 w}{\partial x \partial y},$$
$$Q_x = -D\left(\frac{\partial^3 w}{\partial x^3} + \frac{\partial^3 w}{\partial x \partial y^2}\right), \quad Q_y = -D\left(\frac{\partial^3 w}{\partial x^2 \partial y} + \frac{\partial^3 w}{\partial y^3}\right), \tag{2}$$

where $D = Eh^3/12(1-v^2)$ is the flexural rigidity. The equivalent shear forces are defined by

$$V_x = -D\left[\frac{\partial^3 w}{\partial x^3} + (2-v)\frac{\partial^3 w}{\partial x \partial y^2}\right], \quad V_y = -D\left[(2-v)\frac{\partial^3 w}{\partial x^2 \partial y} + \frac{\partial^3 w}{\partial y^3}\right] \tag{3}$$

2.2. State equation and solution

For the sake of computational efficiency, the following dimensionless variables are used: $V_x = DV_\xi/a$, $V_y = DV_\eta/b$, $M_x = DM_\xi$, $M_y = DM_\eta$, $M_{xy} = DM_{\xi\eta}$, $\xi = x/a$, and $\eta = y/b$. Further, a new variable θ,

$$\theta = \frac{\partial w}{\partial \eta}, \tag{4}$$

i.e. the slope in y direction, is introduced. Following the state space approach [20], one can derive the following state equation with respect to the coordinate η:

$$\frac{\partial}{\partial \eta}\begin{Bmatrix} w \\ \theta \\ M_\eta \\ V_\eta \end{Bmatrix} = \begin{bmatrix} 0 & 1 & 0 & 0 \\ -\dfrac{v\,\partial^2}{s^2 \partial \xi^2} & 0 & -b^2 & 0 \\ 0 & \dfrac{2(1-v)\,\partial^2}{a^2 \quad \partial \xi^2} & 0 & 1 \\ \dfrac{1-v^2}{a^2 s^2}\dfrac{\partial^4}{\partial \xi^4} + \dfrac{\rho h}{D} b^2 \dfrac{\partial^2}{\partial t^2} & 0 & -\dfrac{v\,\partial^2}{s^2 \partial \xi^2} & 0 \end{bmatrix} \begin{Bmatrix} w \\ \theta \\ M_\eta \\ V_\eta \end{Bmatrix}, \tag{5}$$

where $s = a/b$ is the aspect ratio.

Since the current rectangular plate is simply supported at the two opposite edges OB and AC and in harmonic motion, it is assumed that

$$\begin{Bmatrix} w(\xi,\eta) \\ \theta(\xi,\eta) \\ M_\eta(\xi,\eta) \\ V_\eta(\xi,\eta) \end{Bmatrix} = \begin{Bmatrix} \bar{w}(\eta) \\ \bar{\theta}(\eta) \\ \bar{M}_\eta(\eta) \\ \bar{V}_\eta(\eta) \end{Bmatrix} \sin(n\pi\xi)\mathrm{e}^{\mathrm{i}\omega t}, \tag{6}$$

where n is the half-wave number in the x direction, ω the circular frequency, and $\mathrm{i} = \sqrt{-1}$ the imaginary unit. Substitution of Eq. (6) into Eq. (5) yields

$$\frac{\mathrm{d}}{\mathrm{d}\eta}\boldsymbol{\delta}(\eta) = \mathbf{A}(\Omega)\cdot\boldsymbol{\delta}(\eta), \tag{7}$$

where $\boldsymbol{\delta}(\eta) = \left[\bar{w}(\eta) \quad \bar{\theta}(\eta) \quad \bar{M}_\eta(\eta) \quad \bar{V}_\eta(\eta)\right]^{\mathrm{T}}$ is called the state vector, with superscript 'T' denoting transpose of a matrix. The coefficient matrix $\mathbf{A}(\Omega)$ is obtained as

$$\mathbf{A}(\Omega) = \begin{bmatrix} 0 & 1 & 0 & 0 \\ \frac{v}{s^2}k_n^2 & 0 & -b^2 & 0 \\ 0 & -\frac{2(1-v)}{a^2}k_n^2 & 0 & 1 \\ \frac{1-v^2}{a^2 s^2}k_n^4 - \frac{\pi^4\Omega^2}{a^2 s^2} & 0 & \frac{v}{s^2}k_n^2 & 0 \end{bmatrix}, \tag{8}$$

in which $k_n = n\pi$, and $\Omega = (a^2\omega/\pi^2)\sqrt{\rho h/D}$ is the dimensionless frequency.

According to the theory of matrix, the state vector $\boldsymbol{\delta}(\eta_1)$ at a given point $\eta = \eta_1$ and the state vector $\boldsymbol{\delta}(\eta_2)$ at another point $\eta = \eta_2$ are related in accordance with the following transfer relationship [20]:

$$\boldsymbol{\delta}(\eta_2) = \mathbf{T}(\Omega)\cdot\boldsymbol{\delta}(\eta_1), \tag{9}$$

where $\mathbf{T}(\Omega) = \exp\left[(\eta_2 - \eta_1)\cdot\mathbf{A}(\Omega)\right]$ is called the transfer matrix, and $(\eta_2 - \eta_1)$ can be termed as transfer distance or length.

3. Joint coupling matrices

The global analysis of plate can be implemented by directly using the conventional transfer matrix method (CTMM) expressed in Eq. (9), i.e. eliminating the intermediate state vectors using the conditions at internal supports and establishing a transfer relationship between the state vectors at the rightmost and leftmost edges so that the final equations to be solved are kept in a small scale. However, numerical instability occurs when calculations are performed with fixed precision, as has been encountered by many researchers. Such numerical instability has already been recognized, and several effective methods have been proposed, as discussed by Pestel and Leckie [20]. However, the application of these methods has been limited. For example, the delta matrix method is only applicable to lower-order problems, and the modified transfer matrix method requires inversion of sub-determinants which may still cause numerical instability. An alternative way is to extend the precision in floating point calculation, as was done by Xiang et al. [21]. However, the calculation becomes very inefficient and even intolerable when the length of significant numbers increases.

Intrinsically, the numerical difficulty in calculating the transfer exponential matrix in Eq. (9) is caused by eigenvalues with large positive real part of the coefficient matrix $\mathbf{A}(\Omega)$ in Eq. (8) when the aspect ratio of the transfer span to its perpendicular size is large or the frequency is high. It is easy to show that exponentially growing terms and exponentially decaying terms are simultaneously contained in the state-space solution. When eigenvalues bear large positive real part, the exponentially decaying terms, which should be responsible

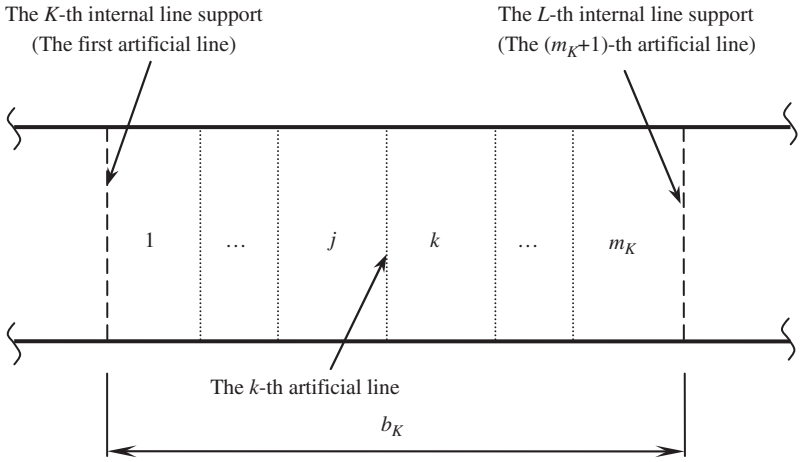

Fig. 2. Division scheme for the Kth span.

for the final results[1], are swamped by the exponentially growing terms, thus making the numerical calculation unstable. For a given frequency, it is clear that the eigenvalues of matrix $\mathbf{A}(\Omega)$ remain unchanged for fixed geometry and material properties because they are unique. However, the exponential of a growing term is also related to the transfer length, as seen from the expression of transfer matrix $\mathbf{T}(\Omega) = \exp\left[(\eta_2 - \eta_1) \cdot \mathbf{A}(\Omega)\right]$. This allows reduction of exponential, and hence avoidance of numerical instability, by shortening the transfer length $(\eta_2 - \eta_1)$ in Eq. (9). Hence, the technique of joint coupling matrices proposed by Nagem and Williams [19] is introduced here to analyze such continuous plates. Although they used the joint coupling matrices and showed the superiority of its numerical efficiency in calculating high frequencies of space structures, Nagem and Williams [19] have not presented an in-depth explanation as discussed in this paper. The current application of joint coupling matrices also differs from Nagem and Williams [19] because artificial line supports should be introduced as shown below.

In practice, a typical span (the Kth span) of the plate is partitioned into m_K sub-spans (segments) by artificial lines parallel to the internal line supports (Fig. 2). Hence the entire continuous plate has a total number of m $(= \sum_{K=1}^{p} m_K)$ sub-spans. All internal line supports, artificial partitioning lines and parallel edges OB and AC are treated as joint lines (or simply, joints), and thus the entire plate has $(m+1)$ joints in total.

At the joint between the last segment of the Jth span and the first segment of the Kth span, i.e. at the Kth rigid line support, the natural and continuity conditions of plate requires

$$\bar{w}_R^{(J)} = 0, \;\; \bar{w}_L^{(K)} = 0, \;\; \bar{\theta}_R^{(J)} = \bar{\theta}_L^{(K)}, \;\; \bar{M}_{\eta R}^{(J)} = \bar{M}_{\eta L}^{(K)}, \;\; \bar{V}_{\eta R}^{(J)} - \bar{V}_{\eta L}^{(K)} = R_K, \tag{10}$$

where superscripts '(J)' and '(K)' denote the adjacent Jth and Kth spans, subscripts 'R' and 'L' represent the right and left ends of a span, and R_K is the vertical reaction force at the Kth line support. The first four conditions in Eq. (10) can be expressed using state vectors into a condensed matrix form as

$$\mathbf{J}_s \begin{Bmatrix} \boldsymbol{\delta}_R^{(J)} \\ \boldsymbol{\delta}_L^{(K)} \end{Bmatrix} = \mathbf{0}, \quad (J = 1, \; 2, \; \ldots, \; p-1, \; K = J+1), \tag{11}$$

in which $\mathbf{J}_s$ is called the joint coupling matrix at the internal line support having explicit expression as

$$\mathbf{J}_s = \begin{bmatrix} 1 & 0 & 0 & 0 & 0 & 0 & 0 & 0 \\ 0 & 0 & 0 & 0 & 1 & 0 & 0 & 0 \\ 0 & 1 & 0 & 0 & 0 & -1 & 0 & 0 \\ 0 & 0 & 1 & 0 & 0 & 0 & -1 & 0 \end{bmatrix}. \tag{12}$$

Note that all joint coupling matrices at the internal rigid line supports are identical as shown in Eq. (12).

[1]This can be easily understood when considering a semi-infinite plate. The growing terms should vanish to satisfy the normality condition at infinity and only the decaying terms are retained in the final expressions of the solution.

At the artificial line joints, the joint coupling relation is established in the same sense as for the internal rigid line supports, but Eq. (10) is now replaced by

$$\bar{w}_R^{(j)} = \bar{w}_L^{(k)}, \ \ \bar{\theta}_R^{(j)} = \bar{\theta}_L^{(k)}, \ \ \bar{M}_{\eta R}^{(j)} = \bar{M}_{\eta L}^{(k)}, \ \ \bar{V}_{\eta R}^{(j)} = \bar{V}_{\eta L}^{(k)}. \tag{13}$$

Rewrite Eq. (13) into a matrix form as

$$\mathbf{J}_a \begin{Bmatrix} \boldsymbol{\delta}_R^{(j)} \\ \boldsymbol{\delta}_L^{(k)} \end{Bmatrix} = \mathbf{0}, \quad (j = 1, \ 2, \ \ldots, \ m_K - 1, \ \ k = j + 1), \tag{14}$$

where $\mathbf{J}_a = \begin{bmatrix} \mathbf{I} & -\mathbf{I} \end{bmatrix}$ is the joint coupling matrix at the artificial line, with $\mathbf{I}$ denoting the identity matrix of 4×4.

Further, edges OA and BC are aslo treated as joints with joint coupling relations as

$$\mathbf{J}_{OA}\boldsymbol{\delta}_L^{(1)} = \mathbf{0}, \ \ \mathbf{J}_{BC}\boldsymbol{\delta}_R^{(p)} = \mathbf{0}, \tag{15}$$

in which $\mathbf{J}_{OA}$ and $\mathbf{J}_{BC}$ depend on supporting conditions of the edges. There are:

Simply supported ($\bar{w} = \bar{M}_\eta = 0$): $\mathbf{J}_e = \begin{bmatrix} 1 & 0 & 0 & 0 \\ 0 & 0 & 1 & 0 \end{bmatrix}$;

Clamped ($\bar{w} = \bar{\theta} = 0$): $\mathbf{J}_e = \begin{bmatrix} 1 & 0 & 0 & 0 \\ 0 & 1 & 0 & 0 \end{bmatrix}$;

Free ($\bar{M}_\eta = \bar{V}_\eta = 0$): $\mathbf{J}_e = \begin{bmatrix} 0 & 0 & 1 & 0 \\ 0 & 0 & 0 & 1 \end{bmatrix}$,

where subscript 'e' is either OA or BC.

4. Frequency equation

General linear analysis for free vibration is presented in this section to establish the governing frequency equation. According to definition of segments and joints in the previous section, there is a total number of m segments and $(m+1)$ joints which consist of $(p-1)$ internal line support joints, $\sum_{K=1}^{p}(m_K - 1)$ artificial line joints and two edge joints. Assembling the $(m+1)$ joint coupling relations in Eqs. (11), (14) and (15), gives the following global joint coupling equation:

$$\mathbf{J}\boldsymbol{\Delta} = \mathbf{0}, \tag{16}$$

where

$$\begin{aligned} &\mathbf{J} = \mathrm{diag}\begin{pmatrix} \mathbf{B}_1 & \cdots & \mathbf{B}_K & \cdots & \mathbf{B}_p & \mathbf{J}_{BC} \end{pmatrix}, \\ &\mathbf{B}_1 = \mathrm{diag}\begin{pmatrix} \mathbf{J}_{OA} & \mathbf{J}_a & \cdots & \mathbf{J}_a \end{pmatrix}, \ \ \mathbf{B}_K = \mathrm{diag}\begin{pmatrix} \mathbf{J}_s & \mathbf{J}_a & \cdots & \mathbf{J}_a \end{pmatrix}, \\ &\boldsymbol{\Delta} = \begin{bmatrix} \begin{Bmatrix} \boldsymbol{\delta}_{1,L} \\ \boldsymbol{\delta}_{1,R} \end{Bmatrix} & \cdots & \begin{Bmatrix} \boldsymbol{\delta}_{i,L} \\ \boldsymbol{\delta}_{i,R} \end{Bmatrix} & \cdots & \begin{Bmatrix} \boldsymbol{\delta}_{m,L} \\ \boldsymbol{\delta}_{m,R} \end{Bmatrix} \end{bmatrix}, \quad (i = 1, \ 2, \ \ldots, \ m). \end{aligned} \tag{17}$$

In the general analysis, $\boldsymbol{\delta}_{i,L}$ and $\boldsymbol{\delta}_{i,R}$ are used to designate state vectors at left and right ends of the ith segment. From the above analysis, the total number of elements of the global state vector $\boldsymbol{\Delta}$ is 8 m and the global joint coupling matrix $\mathbf{J}$ is of dimension $4\,\mathrm{m} \times 8\,\mathrm{m}$.

Eq. (16) contains the information of equilibrium and compatibility at all joints of the continuous plate, but it has no information about the sub-spans. As described in Eq. (9), the state vectors, $\boldsymbol{\delta}_{i,L}$ and $\boldsymbol{\delta}_{i,R}$, respectively, at left and right ends of the ith sub-span, are related by

$$\boldsymbol{\delta}_{i,R} = \mathbf{T}_i(\Omega) \cdot \boldsymbol{\delta}_{i,L}, \quad (i = 1, \ 2, \ldots, \ m). \tag{18}$$

Such equations containing the information of segments should be combined with the global joint coupling relationship. In fact, introducing the following identity equation:

$$\boldsymbol{\delta}_{i,L} = \boldsymbol{\delta}_{i,L}, \tag{19}$$

and combining it with Eq. (18) result in

$$\bar{\boldsymbol{\Delta}} = \mathbf{G}(\Omega) \cdot \boldsymbol{\Delta}_L, \tag{20}$$

where

$$\bar{\boldsymbol{\Delta}} = \begin{Bmatrix} \boldsymbol{\delta}_{1,\mathrm{R}} \\ \boldsymbol{\delta}_{2,R} \\ \vdots \\ \boldsymbol{\delta}_{m,R} \\ \boldsymbol{\delta}_{1,L} \\ \boldsymbol{\delta}_{2,L} \\ \vdots \\ \boldsymbol{\delta}_{m,\mathrm{L}} \end{Bmatrix}, \quad \boldsymbol{\Delta}_L = \begin{Bmatrix} \boldsymbol{\delta}_{1,L} \\ \boldsymbol{\delta}_{2,L} \\ \vdots \\ \boldsymbol{\delta}_{m,L} \end{Bmatrix}, \quad \mathbf{G}(\Omega) = \begin{bmatrix} \mathbf{T}_1(\Omega) & & & \\ & \mathbf{T}_2(\Omega) & & \\ & & \ddots & \\ & & & \mathbf{T}_m(\Omega) \\ \mathbf{I} & & & \\ & \mathbf{I} & & \\ & & \ddots & \\ & & & \mathbf{I} \end{bmatrix}. \tag{21}$$

In Eq. (21), $\bar{\boldsymbol{\Delta}}$ contains all state vectors of the m segments, while $\boldsymbol{\Delta}_L$ contains state vectors only at the left ends of all segments. The matrix entries not shown in $\mathbf{G}(\Omega)$ are zero.

Recall that the vector $\boldsymbol{\Delta}$ in Eq. (17) contains the same elements as $\bar{\boldsymbol{\Delta}}$, but in a different sequence. Then, introduce the following permutation relationship:

$$\boldsymbol{\Delta} = \mathbf{P}\bar{\boldsymbol{\Delta}}, \tag{22}$$

where the matrix $\mathbf{P}$ is a permutation matrix with each column and each row having only one identity element. It is obvious that matrix $\mathbf{G}(\Omega)$ is of dimension $8\,\mathrm{m} \times 4\,\mathrm{m}$ and the permutation matrix $\mathbf{P}$ is of dimension $8\,\mathrm{m} \times 8\,\mathrm{m}$. Substituting Eq. (20) into Eq. (22) and further eliminating $\boldsymbol{\Delta}$ from Eq. (16) yield

$$\mathbf{JPG}(\Omega) \cdot \boldsymbol{\Delta}_L = \mathbf{0}, \tag{23}$$

where the product matrix JPG(Ω) is of dimension $4\,\mathrm{m} \times 4\,\mathrm{m}$. For free vibration, the non-trivial solution of Eq. (23) requires the determinant of the coefficient matrix to vanish, i.e.

$$Q = \left|\mathbf{JPG}(\Omega)\right| = 0, \tag{24}$$

which is the governing frequency equation. It should be pointed out that the frequency equation can be established in an alternative way, see Appendix A. The difference of the latter formalism from Eq. (23) is also discussed in Appendix A.

After obtaining the frequency from Eq. (24), the state vectors at all joints can be determined with respect to an arbitrary factor. The last equation in Eq. (10) is then used to determine the vertical reaction forces at the rigid line supports.

5. Numerical results and discussion

In order to illustrate efficiency of the present approach, a rectangular plate with internal rigid line supports (Fig. 1), with Poisson's ratio $v = 0.3$ is considered here. For convenience, "$XSYS$" is adopted to denote boundary conditions at all four edges of the plate. The character S denotes simply supported conditions at the two opposite edges while characters X and Y, respectively, correspond to edges OA and BC, may be clamped (C), simply supported (S) or free (F). The validation, efficiency study compared with CTMM, and influence of location of internal line supports on natural frequencies are considered in sequence. The dimensionless frequency Ω is searched based on Eq. (24) using the bisection method with step length $\Delta\Omega = 0.001$ and precision $\pm 10^{-8}$.

5.1. Validation of the method

A three-unequal span continuous rectangular plate is considered to validate the present hybrid method of state space formulations and joint coupling matrices. The plate has an aspect ratio of $b/a = 4$, and a span layout of $b_1 = b_3 = b/4$ and $b_2 = b/2$. No division of spans is necessary in this example, and hence the total segment number is 3. Numerical results for the first six dimensionless frequencies for different combinations of boundary conditions are calculated and tabulated in Table 1. For validation, FEM results are also presented, which are calculated using Shell63 elements with lengths of $0.02a \times 0.02a$ in the software ANSYS9.0. It is observed that the present numerical results are identical to FEM results and those reported by Azimi et al. [9] and Xiang et al. [18]. This verifies the derivation as well as programming in this paper.

5.2. Comparison with CTMM

In order to illustrate the superior efficiency of this method over CTMM, the highest-order frequency that can be predicted numerically for a fully simply supported (*SSSS*) single-span rectangular plate having an aspect ratio of $b/a = 6$ is investigated. For single-span isotropic plate, it should be noted that the final transfer relationship of state vectors at left and right edges of plate remains identical in CTMM regardless of how many segments taken in the calculation:

$$\boldsymbol{\delta}(1) = \mathbf{T}(\Omega) \cdot \boldsymbol{\delta}(0), \tag{25}$$

where $\mathbf{T}(\Omega) = \exp[\mathbf{A}(\Omega)]$ is the global transfer matrix. Introducing boundary conditions at edges OA and BC and for non-trivial free vibration solution, the following frequency equation is obtained:

$$\begin{vmatrix} T_{12} & T_{14} \\ T_{32} & T_{34} \end{vmatrix} = 0, \tag{26}$$

where T_{ij} are elements of the matrix $\mathbf{T}(\Omega)$. In the joint coupling matrices method, it is obvious that the final frequency equation, i.e. Eq. (24), is exactly the same as Eq. (26) if only one segment is taken (i.e. no division of span). Hence, the numerical result of CTMM is expected to be exactly the same as that of the present method with one segment (sub-span).

Fig. 3 shows the curves of determinant value Q versus dimensionless frequency Ω for the highest-order natural frequency that can be predicted using a given m (equal-length division) for mode number $n = 1$ in Eq. (6). By increasing m, it is seen from Fig. 3 that natural frequencies of higher-order can be obtained, and CTMM can only predict a small number of natural frequencies corresponding to $m = 1$. Table 2 presents the numerically predictable highest-order dimensionless frequencies for different sub-span numbers. For a fully simply supported plate, Leissa [22] presented a simple analytical form of natural frequencies as

Table 1
Comparison of natural frequency parameter (Ω) of a three-unequal span continuous rectangular plate

B.C. type	Sources	Mode number					
		1	2	3	4	5	6
SSSS	Present	1.30893	2.00000	2.18181	2.39587	3.56766	4.27977
	FEM	1.3088	1.9998	2.1816	2.3955	3.5669	4.2792
	[18]	1.3089	2.0000	2.1818	2.3959	3.5677	4.2798
	[9]	1.3091	2.0000	2.1814	2.3962	3.5675	4.2798
CSSS	Present	1.31088	2.03623	2.29402	2.68483	3.60634	4.28004
	FEM	1.3108	2.0360	2.2937	2.6844	3.6056	4.2796
	[18]	1.3109	2.0362	2.2940	2.6848	3.6063	4.2800
	[9]	1.3111	2.0366	2.2939	2.6850	3.6060	4.2798
CSCS	Present	1.3129	2.1088	2.5978	2.7479	3.6442	4.2803
	FEM	1.3128	2.1086	2.5973	2.7473	3.6435	4.2798
	[9]	1.3131	2.1085	2.5979	2.7478	3.6445	4.2808

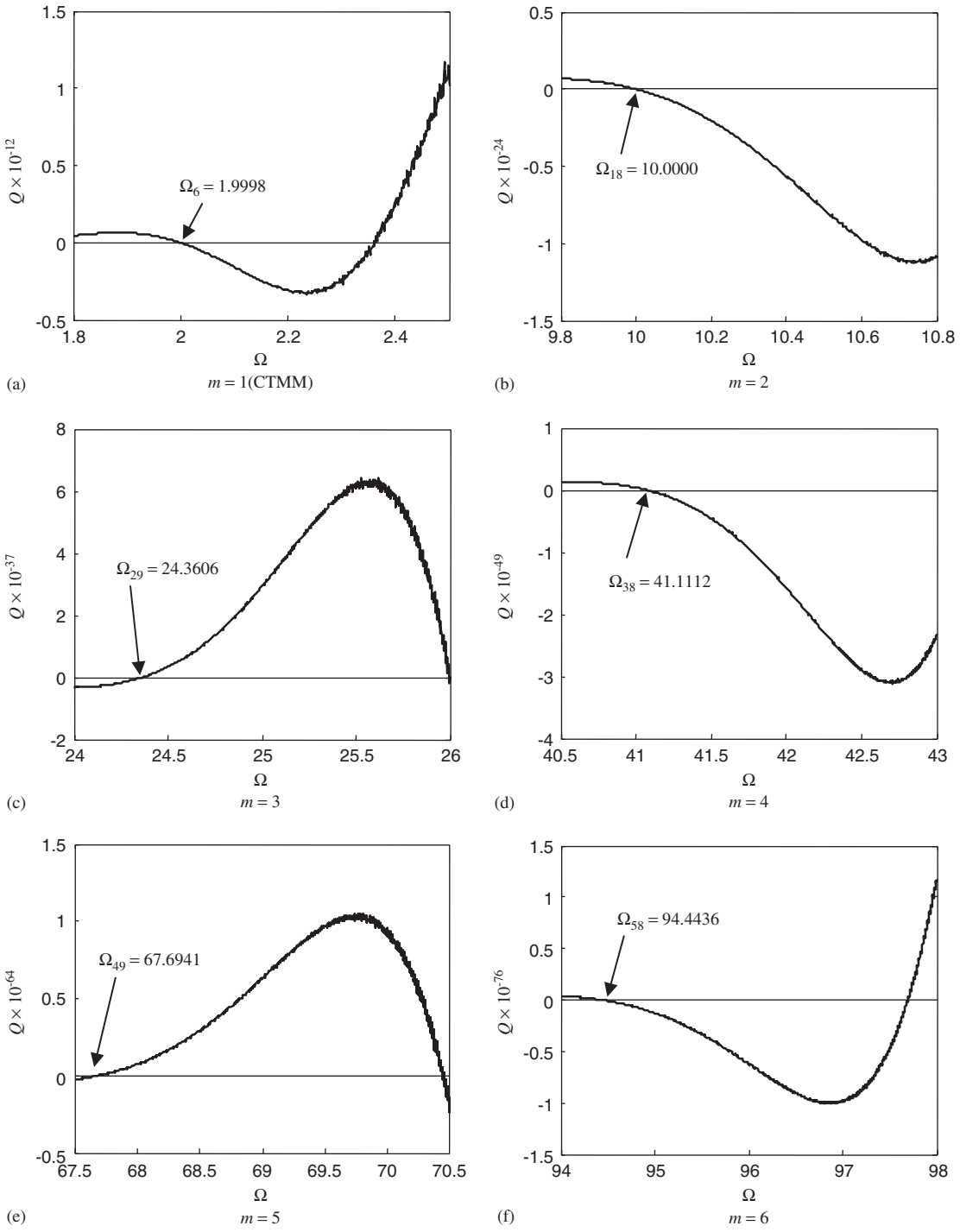

Fig. 3. Curves of the determinant Q versus the frequency parameter Ω around the numerically predictable highest-order natural frequency ($n = 1$).

$\Omega_{n_y} = 1 + n_y^2/36$ (n_y is the mode number in y direction). There is evidence that the predictable number of frequencies increases with the number of sub-spans. This table also serves as a convergence study of the present method. It is seen that the highest-order frequency for a special sub-span number m can be obtained with high

Table 2
Convergence study for the numerically predictable highest-order natural frequency of an *SSSS* single-span rectangular plate ($n = 1$)

m	Ω_6	Ω_{18}	Ω_{29}	Ω_{38}	Ω_{49}	Ω_{58}
1	1.9998	—	—	—	—	—
2	2.0000	10.0000	—	—	—	—
3	2.0000	10.0000	24.3606		—	—
4	2.0000	10.0000	24.3611	41.1112	—	—
5	2.0000	10.0000	24.3611	41.1111	67.6941	—
6	2.0000	10.0000	24.3611	41.1111	67.6945	94.4436
[22]	2.0000	10.0000	24.3611	41.1111	67.6944	94.4444

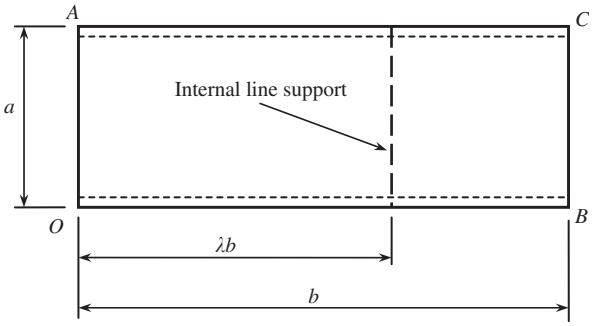

Fig. 4. A rectangular plate with one internal line support.

accuracy although the curve in Fig. 3 subsequently oscillates sharply. The present results are identical to the analytical results of Leissa [22]. Accuracy of results and numerical stability can be really enhanced by increasing the sub-span number but with a sacrifice of computational time. Through this example, it is illustrated that one can calculate an arbitrary high-order frequency by taking a proper number of sub-spans. This is however impossible when the conventional formalism of transfer matrix method is employed.

5.3. *Effect of the internal line supports location*

A two-span plate is depicted in Fig. 4. The position of the intermediate line support is indicated by a location parameter λ. Effect of this parameter λ on the natural frequencies of a long-span continuous plate is investigated.

Fig. 5 exhibits the variations of the first five frequency parameters Ω versus the location parameter λ for a rectangular plate with one internal line support and an aspect ratio $b/a = 14$. The location of the intermediate support is shifted from left ($\lambda = 0.001$) to the center ($\lambda = 0.5$) for symmetric plates (i.e. *CSCS*, *SSSS* and *FSFS*), and to right ($\lambda = 0.999$) for asymmetric plates (i.e. *CSSS*, *CSFS* and *SSFS*). The step length in calculation is taken as $\Delta\lambda = 0.001$ for line support near edges and $\Delta\lambda = 0.01$ for support elsewhere, as can be seen from Fig. 5.

It is observed from Figs. 5(a)–(c) that for symmetric plates, the frequency parameter Ω of the first mode increases monotonically when the internal line support moves from the plate edge ($\lambda = 0.001$) to the plate center ($\lambda = 0.5$). Thus for symmetric plates, locating the internal line support at the plate center maximizes the fundamental frequency, a considerable significance in engineering practice. For *CSSS* plate, the optimal location (corresponding to the largest fundamental frequency) of support is also near $\lambda = 0.5$, while for the other two asymmetric (i.e. *CSFS* and *SSFS*) plates, the optimal locations of internal line support move towards the free edge, both at about $\lambda = 0.73$.

For a specific order of frequency, it is seen from Fig. 5 that the number of optimal locations (corresponding to high frequencies that are nearly equal) is the same as the order of frequency. This should be the case when

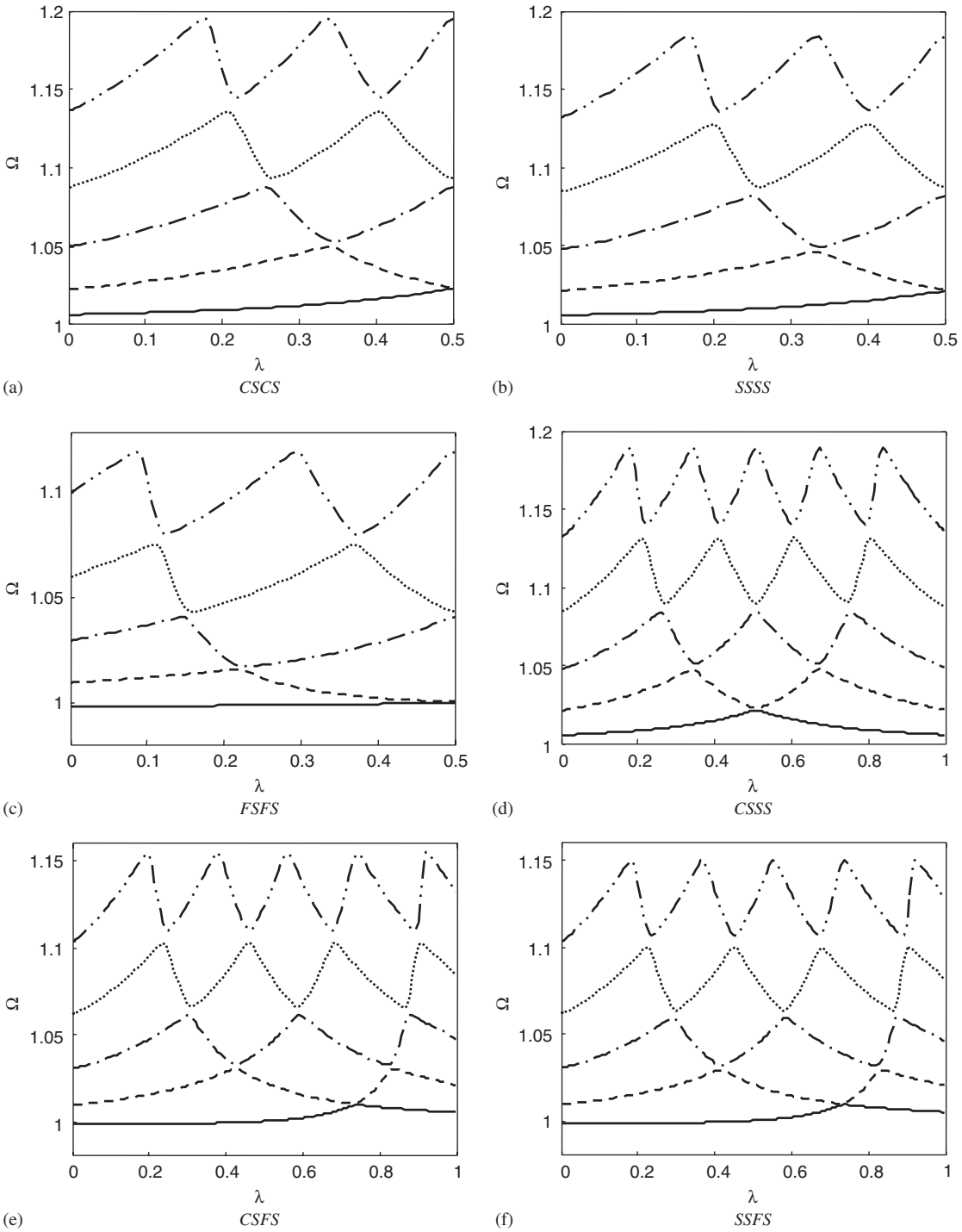

Fig. 5. Variation of frequency parameter Ω versus location parameter λ for a two-span rectangular plate ($b/a = 14$).

considering the shape of a particular vibration mode of the corresponding single-span plate. For example, for the second vibration mode, there are two positions having the most significant vibration amplitude. Hence there exist two optimal positions for imposing internal rigid line supports to enhance frequency corresponding to this mode. Note that the optimal positions may not exactly coincide with those locations where the

Table 3
Comparison of the first six frequency parameters Ω of a two-span plate with a small location parameter ($\lambda = 0.001$) with those of the corresponding single-span plate

B.C. type	Mode 1	Mode 2	Mode 3	Mode 4	Mode 5	Mode 6
SSCS (2)	1.00545	1.02180	1.04902	1.08707	1.13589	1.19541
CSCS (1)	1.00545	1.02177	1.04896	1.08695	1.13570	1.19514
FSCS (2)	1.00529	1.02115	1.04756	1.08451	1.13196	1.18989
SSSS (2)[a]	1.00528	1.02110	1.04747	1.08435	1.13172	1.18955
SSCS (1)	1.00527	1.02108	1.04740	1.08423	1.13154	1.18929
FSSS (2)	1.00512	1.02048	1.04607	1.08190	1.12796	1.18425
SSSS (1)	1.00510	1.02041	1.04592	1.08163	1.12755	1.18367
SSFS (2)	0.99830	1.00976	1.03059	1.06182	1.10340	1.15529
CSFS (1)	0.99830	1.00974	1.03055	1.06173	1.10326	1.15508
FSFS (2)	0.99829	1.00944	1.02966	1.05999	1.10041	1.15090
SSFS (1)	0.99829	1.00941	1.02956	1.05980	1.10009	1.15043

[a]Denotes the results computed for a plate with $\lambda = 0.999$.

vibration amplitude of a single-span plate is the largest. This is because introducing a rigid line support into a single-span plate changes the dynamic behavior of plate to a certain extent.

The optimal locations distributed symmetrically with respect to the plate centeral line for a symmetric plate. When the internal line support moves towards simply supported edge or free edge ($\lambda = 0.001$), the plate behaves like a single-span one with the corresponding edge being clamped or simply supported. This is further confirmed through numerical comparison in Table 3, where the first six frequency parameters Ω of a two-span plate with a small location parameter ($\lambda = 0.001$) are compared with those of the single-span plate but with the corresponding shifted edge supports. The number in parenthesis of boundary conditions represents a two-span plate (2) or a single-span plate (1). It is seen that the two-span *FSCS* and *SSSS* plates behave like the single-span *SSCS* plate when the internal line support is located very near to the left ($\lambda = 0.001$) and the right ($\lambda = 0.999$) edges, respectively. This is reasonable because when the line support is very close to a simple support, a constraint on the slope is likely to occur there, and hence the two supports serve as a single clamped one. Similar argument can be stated for the case with a line support moves towards a free edge.

6. Conclusions

A free vibration analysis based on the exact solution of rectangular Kirchhoff plate with two opposite simply supported edges and internal line supports is presented. To avoid numerical instability frequently encountered in the CTMM for a long transfer distance or for high frequency, each span is further divided into several sub-segments. In addition, the joint coupling matrices concept is employed to group the boundary conditions at two edges and the continuity conditions at the internal line supports as well as artificial lines.

The proposed method has been validated through well conducted comparison with established results. The effectiveness of using joint coupling matrices is studied by considering a single-span plate having a large aspect ratio. It is shown that both numerical stability and accuracy can be significantly improved when compared to the CTMM.

Influence of the internal line support position on the natural frequencies of a two-span plate with a large aspect ratio has been investigated. The location parameter can be optimized to improve the fundamental frequency. When the internal line support is very near to the simply supported or free edge, the edge behaves like a clamped or simply supported one.

Acknowledgments

The work described in this paper was partly supported by the National Natural Science Foundation of China (No. 10432030) and partly by the Research Grants Council of the Hong Kong Special Administrative Region (Project No. 9040683 CityU 1032/02E).

Appendix A. An alternative way to derive the frequency equation

Eq. (18) can be rearranged as

$$\left[\mathbf{T}_i(\Omega) \quad -\mathbf{I}\right] \cdot \begin{Bmatrix} \boldsymbol{\delta}_{i,L} \\ \boldsymbol{\delta}_{i,R} \end{Bmatrix} = \mathbf{0}, \quad (i = 1,\ 2, \ldots,\ m). \tag{A.1}$$

Assembling all transfer relationships in Eq. (A.1) yields

$$\mathbf{H}(\Omega) \cdot \boldsymbol{\Delta} = \mathbf{0}, \tag{A.2}$$

where

$$\mathbf{H}(\Omega) = \begin{bmatrix} \mathbf{T}_1(\Omega) & -\mathbf{I} & & & & \\ & & \mathbf{T}_2(\Omega) & -\mathbf{I} & & \\ & & & & \ddots & \\ & & & & & \mathbf{T}_m(\Omega) \end{bmatrix}, \tag{A.3}$$

Grouping Eq. (16) and Eq. (A.2) results in

$$\begin{bmatrix} \mathbf{J} \\ \mathbf{H}(\Omega) \end{bmatrix} \cdot \boldsymbol{\Delta} = \mathbf{0}, \tag{A.4}$$

where the coefficient matrix is of dimension $8\,\mathrm{m} \times 8\,\mathrm{m}$. The requirement for non-trivial solution of Eq. (A.4) leads to the following frequency equation:

$$\bar{Q} = \left| \begin{bmatrix} \mathbf{J} \\ \mathbf{H}(\Omega) \end{bmatrix} \right| = 0. \tag{A.5}$$

Obviously, the dimension of $\left[\mathbf{J}^{\mathrm{T}}\ \mathbf{H}^{\mathrm{T}}\right]^{\mathrm{T}}$ is double to that of matrix $\mathbf{JPG}(\Omega)$, but no matrix multiplication is involved in the former. Numerical test shows that Eqs. (24) and (A.5) yield exactly identical results. It is noted that the global state vector $\boldsymbol{\Delta}$ contains many repetitive state vectors at the common artificial line of two adjacent segments, as can be seen from Eq. (14). This makes it uneconomical for storage when computing natural frequencies and normal modes of plate.

References

[1] A.S. Veletsos, N.M. Newmark, Determination of natural frequencies of continuous plates hinged along two opposite edges, *ASME, Journal of Applied Mechanics* 23 (1956) 97–102.

[2] E.E. Ungar, Free oscillations of edge-connected simply supported plate systems, *ASME, Journal of Engineering for Industry* 83 (1961) 434–440.

[3] S.M. Dickinson, G.B. Warburton, Natural frequencies of plate systems using the edge-effect method, *Journal of Mechanical Engineering Science* 9 (1967) 318–329.

[4] Y.K. Cheung, M.S. Cheung, Flexural vibrations of rectangular and other polygonal plates, *ASCE, Journal of the Engineering Mechanics Division* 97 (1971) 391–411.

[5] C.I. Wu, Y.K. Cheung, Frequency analysis of rectangular plates continuous in one or two directions, *Earthquake Engineering and Structural Dynamics* 3 (1974) 3–14.

[6] B.W. Golley, J. Petrolito, Finite strip-elements for the dynamic analysis of orthotropic plate structures, *Journal of Sound and Vibration* 163 (1993) 479–491.

[7] T. Sakata, A reduction method for vibrating and buckling problems of orthotropic continuous plates, *Journal of Sound and Vibration* 49 (1976) 45–52.
[8] K. Takahashi, T. Chishaki, Free vibrations of two-way continuous rectangular plates, *Journal of Sound and Vibration* 62 (1979) 455–459.
[9] S. Azimi, J.F. Hamilton, W. Soedel, The receptance method applied to the free vibration of continuous rectangular plates, *Journal of Sound and Vibration* 93 (1984) 9–29.
[10] R.E.D. Bishop, D.C. Johnson, *The Mechanics of Vibration*, Cambridge University Press, London, 1960.
[11] V.H. Cortinez, P.A.A. Laura, A note on vibrating membranes and plates with an internal support, *Journal of Sound and Vibration* 104 (1986) 533–535.
[12] S.C. Kim, S.M. Dickinson, The flexural vibration of line supported rectangular plate systems, *Journal of Sound and Vibration* 114 (1987) 129–142.
[13] K.M. Liew, K.Y. Lam, Vibration analysis of multi-span plates having orthogonal straight edges, *Journal of Sound and Vibration* 147 (1991) 255–264.
[14] K.M. Liew, Y. Xiang, S. Kitipornchai, Transverse vibration of thick rectangular plates—II. Inclusion of oblique internal line supports, *Computers and Structures* 49 (1993) 31–58.
[15] D. Zhou, Eigenfreqeuncies of line supported rectangular plates, *International Journal of Solids and Structures* 31 (1994) 347–358.
[16] J. Kong, Y.K. Cheung, Vibration of shear-deformable plates with intermediate line supports: a finite layer approach, *Journal of Sound and Vibration* 184 (1995) 639–649.
[17] G.W. Wei, Y.B. Zhao, Y. Xiang, Discrete singular convolution and its application to the analysis of plates with internal supports, part 1: theory and algorithm, *International Journal for Numerical Methods in Engineering* 55 (2002) 913–946.
[18] Y. Xiang, Y.B. Zhao, G.W. Wei, Levy solutions for vibration of multi-span rectangular plates, *International Journal of Mechanical Sciences* 44 (2002) 1195–1218.
[19] R.J. Nagem, J.H. Williams, Dynamic analysis of large space structures using transfer matrices and joint coupling matrices, *Mechanics of Structures and Machines* 17 (1989) 349–371.
[20] E.C. Pestel, F.A. Leckie, *Matrix Methods in Elastomechanics*, McGraw-Hill, New York, 1963.
[21] Y. Xiang, K.M. Liew, S. Kitipornchai, Exact buckling solutions for composite laminates: proper free edge conditions under in-plane loadings, *Acta Mechanica* 117 (1996) 115–128.
[22] A.W. Leissa, *Vibration of plates, NASA SP-160. Office of Technology Untilization*, NASA, Washington D.C, 1969.